

Direct synthesis of hydrogen peroxide from H₂ and O₂ using TiO₂-supported Au–Pd catalysts

Jennifer K. Edwards^a, Benjamin E. Solsona^a, Philip Landon^a, Albert F. Carley^a, Andrew Herzing^b, Christopher J. Kiely^b, Graham J. Hutchings^{a,*}

^a School of Chemistry, Cardiff University, Main Building, Park Place, Cardiff, CF10 3AT, UK

^b Center for Advanced Materials and Nanotechnology, Lehigh University, 5 East Packer Avenue, Bethlehem, PA 18015-3195, USA

Received 1 July 2005; revised 1 September 2005; accepted 6 September 2005

Available online 17 October 2005

Abstract

The direct synthesis of H₂O₂ at low temperature (2 °C) from H₂ and O₂ using TiO₂-supported Au, Pd, and Au–Pd catalysts is discussed. The Au–Pd catalysts performed significantly better than the pure Pd/TiO₂ and Au/TiO₂ materials. Au–Pd particles were found with a core–shell structure, with Pd concentrated on the surface. The highest yields of H₂O₂ were observed with uncalcined catalysts, but these were particularly unstable, losing both metals during use. In contrast, samples calcined at 400 °C were stable and could be reused several times without loss of performance. These catalysts exhibited low activity for CO oxidation at 25 °C; conversely, catalysts effective for low-temperature CO oxidation were inactive for H₂ oxidation to H₂O₂. This anticorrelation is explored in terms of the mechanism by which the catalysts function and the design of catalysts for the selective oxidation of one of these substrates in the presence of the other.

© 2005 Elsevier Inc. All rights reserved.

Keywords: Hydrogen peroxide; Selective oxidation; CO oxidation; Bimetallic catalysts; Gold; Palladium; Titania; XPS; TEM; Core–shell particles

1. Introduction

Oxidation is a key process that can be used either to functionalise molecules using selective or partial oxidation or to remove pollutants using nonselective or total oxidation. Increasing attention is being given to green chemical reactions, which focuses interest on the design of chemical processes that are atom-efficient. This is particularly true in the fine chemicals industry, where many reactions are operated with low atom efficiency. In this respect, oxidation reactions exhibit significant problems, because stoichiometric (i.e., noncatalytic) processes are often used with a range of oxygen donors [1]. Molecular oxygen is the preferred oxidant [2], but to date, although well exploited in the bulk and petrochemical industries, remarkably

few processes are operating using O₂ as the oxidant. Indeed, many processes use bulky stoichiometric oxygen donors (e.g., sodium perborate, sodium percarbonate, metallic peroxides, organic hydroperoxides, percarboxylic acids), which inherently exhibit poor atom efficiency [3–6]. One problem is that dioxygen has a triplet ground state, whereas the organic substrates typically have singlet ground states; consequently, activation of the substrate is required, and often the temperatures required to achieve this are excessive for the reactions of interest in the synthesis of fine chemicals. From a green chemistry perspective, hydrogen peroxide is the next most preferred oxidant, because water is the byproduct after oxygen donation. In view of this, there is significant interest in using hydrogen peroxide as an oxygen source, which has brought renewed efforts in both the synthesis and use of hydrogen peroxide. In this paper we address the use of highly efficient gold-based catalysts for the direct synthesis of hydrogen peroxide from the reaction of H₂ and O₂.

Hydrogen peroxide is a noted green oxidant that has widespread applications in many large-scale processes, including

* Corresponding author. Fax: +44 29 2087 4030.

E-mail addresses: edwardsjk@cf.ac.uk (J.K. Edwards), bensoles@yahoo.es (B.E. Solsona), landonp@cf.ac.uk (P. Landon), carley@cf.ac.uk (A.F. Carley), aah5@lehigh.edu (A. Herzing), chris.kiely@lehigh.edu (C.J. Kiely), hutch@cardiff.ac.uk (G.J. Hutchings).

as bleaching [7] and disinfecting. Such uses account for the majority of the H_2O_2 material manufactured. Its use in the fine chemical industry accounts for a much lower fraction of its consumption (e.g., epoxidised oils, catechol, hydroquinone, peracetic acid, caprolactone) and tends to require only small amounts. The discovery of the titanium silicalite TS-1 [8] and its application for the oxidation of propene to propene oxide and the ammoxidation of cyclohexanone to its oxime using hydrogen peroxide has triggered more interest in using hydrogen peroxide for the synthesis of chemical intermediates.

At present, hydrogen peroxide is produced by the sequential hydrogenation and oxidation of an alkyl anthraquinone [9]. However, there are problems associated with the anthraquinone route, including the cost of the quinone solvent system and the requirement for periodic replacement of anthraquinone due to hydrogenation. In addition, the process is economically viable only on a relatively large scale ($4\text{--}6 \times 10^4$ TPa). This necessitates the transportation and storage of concentrated solutions of hydrogen peroxide when required for use in the fine chemicals industry, because only relatively small amounts are required at any one time. Hence the development of a new, highly efficient, and smaller-scale manufacturing process for H_2O_2 is of significant commercial interest.

The identification of a direct route for the synthesis of hydrogen peroxide from the reaction of dioxygen and hydrogen would be highly beneficial, because this presents the tantalizing possibility of small-scale-distributed synthesis. At present, no commercial process exists for the direct process, even though there has been significant interest in this reaction in industrial laboratories for more than 90 years [10–28]. Until very recently, the catalysts used in these investigations have been based on Pd. Because it is important to try to achieve the highest rate of product formation, most of these earlier studies used H_2/O_2 mixtures in the explosive region, and solutions of >35 wt% hydrogen peroxide have been made by reacting H_2/O_2 over Pd catalysts at elevated pressures [29]. However, operating commercially in the explosive region would be considered extremely dangerous, and thus more recent studies have concentrated on carrying out the reaction with dilute H_2/O_2 mixtures well away from the explosive regime [19,22].

In earlier papers concerning the direct synthesis of H_2O_2 , we showed that catalysts based on Au–Pd alloys supported on alumina can provide a significantly improved rate of hydrogen peroxide formation compared with the Pd-only catalyst [28, 29]. However, in common with pure Pd catalysts, these Al_2O_3 -supported Au–Pd alloys gave low selectivity based on H_2 . This represents the key problem that remains to be solved, because the conditions that are required to produce hydrogen peroxide also promote (i) its decomposition to oxygen and water, (ii) its hydrogenation to water, or (iii) the direct nonselective formation of water.

In this paper we extend our initial studies [28,29] and report a detailed investigation of Au–Pd catalysts supported on TiO_2 , using dilute H_2/O_2 mixtures below the lower explosion limit. With these catalysts, we can now obtain high rates of hydrogen peroxide formation combined with high selectivity and

conversion based on hydrogen, such that these materials can be considered as the starting point for commercialisation.

2. Experimental

2.1. Catalyst preparation

Here 5 wt% Pd/ TiO_2 , 5 wt% Au/ TiO_2 , and a range of Au–Pd/ TiO_2 catalysts were prepared by impregnation of TiO_2 (Degussa P25, mainly anatase) via an incipient wetness method using aqueous solutions of PdCl_2 (Johnson Matthey) and/or $\text{HAuCl}_4 \cdot 3\text{H}_2\text{O}$ (Johnson Matthey). For the 2.5% Au/2.5% Pd/ TiO_2 catalyst, the detailed procedure was as follows. An aqueous solution of $\text{HAuCl}_4 \cdot 3\text{H}_2\text{O}$ [10 ml, 5 g dissolved in water (250 ml)] and an aqueous solution of PdCl_2 [4.15 ml, 1 g in water (25 ml)] were simultaneously added to TiO_2 (3.8 g). The paste formed was ground and dried at 80°C for 16 h and calcined in static air, typically at 400°C for 3 h, although other heat treatment conditions have been investigated. Other Au–Pd ratios were prepared by varying the amounts of starting reagents accordingly.

An additional series of catalysts containing 5 wt% Au on TiO_2 were prepared by deposition precipitation. For 5 wt% Au/ TiO_2 an aqueous solution of $\text{HAuCl}_4 \cdot 3\text{H}_2\text{O}$ [20 ml, 5 g dissolved in water (250 ml)] was added to a solution of TiO_2 in water (3.9 g, 150 ml). This solution was stirred at room temperature for 10 min, and then a solution of NaOH in water (1 g, 25 ml) was added dropwise until the pH of the solution reached 9. The solution was stirred and maintained at pH 9 for 60 min. The catalyst was then washed, filtered, and dried at 80°C for 16 h.

The catalysts prepared by impregnation or deposition–precipitation were pretreated using a range of conditions: drying at 120°C in air, calcination in static air at 200°C for 3 h, calcination in static air at 400°C for 3 h, and reduction in flowing H_2 (5 wt% H_2 in Ar) at 500°C .

2.2. Catalyst testing

2.2.1. Hydrogen peroxide synthesis

Catalyst testing was performed using a stainless steel autoclave (Parr Instruments) with a nominal volume of 50 ml and a maximum working pressure of 14 MPa. The autoclave was equipped with an overhead stirrer (0–2000 rpm) and provisions for measuring temperature and pressure. Typically, the autoclave was charged with the catalyst (0.01 g unless otherwise stated) and solvent (5.6 g MeOH and 2.9 g H_2O), purged three times with CO_2 (3 MPa), and then filled with 5% H_2/CO_2 and 25% O_2/CO_2 to give a hydrogen-to-oxygen ratio of 1:2 at a total pressure of 3.7 MPa. Stirring (1200 rpm unless otherwise stated) was started after reaching the desired temperature (2°C), and experiments were carried out for 30 min unless otherwise stated. Gas analysis for H_2 and O_2 was performed by gas chromatography using a thermal conductivity detector and a CP–Carboplot P7 column (25 m, 0.53 mm i.d.). Conversion of H_2 was calculated by gas analysis before and after reaction. H_2O_2 yield was determined by titration of aliquots

of the final filtered solution with acidified $\text{Ce}(\text{SO}_4)_2$ ($7 \times 10^{-3} \text{ mol l}^{-1}$). $\text{Ce}(\text{SO}_4)_2$ solutions were standardised against $(\text{NH}_4)_2\text{Fe}(\text{SO}_4)_2 \cdot 6\text{H}_2\text{O}$ using ferroin as an indicator.

Methanol was chosen as the solvent because it aids H_2 solubility but does not form peroxides, unlike the higher alcohols. Moreover, the reaction with water alone was found to be less effective. CO_2 was used as the inert gas because the explosive region for H_2/O_2 mixtures is much narrower than for other inert gases.

2.2.2. CO oxidation

The catalytic activity for CO oxidation was determined in a fixed-bed quartz microreactor, operated at atmospheric pressure. The feed consisted of $\text{CO}/\text{O}_2/\text{N}_2$ with a molar ratio of 0.5/19.9/79.6. The combined flow rate was maintained at 22.5 ml min^{-1} , and a constant catalyst loading of 50 mg was used. The catalyst temperature was maintained at 25°C by immersing the quartz bed in a thermostatically controlled water bath. Catalysts were tested for a minimum of 500 min, and analysis of the reaction product was carried out using on-line gas chromatography. Conversion was calculated on the basis of CO_2 concentration in the effluent, and carbon balances were $100 \pm 2\%$.

2.3. Catalyst characterisation

Catalysts were characterised by powder X-ray diffraction (XRD) using an Enraf Nonius PSD120 diffractometer with a monochromatic $\text{Cu-K}\alpha_1$ source operated at 40 keV and 30 mA. Phases were identified by matching experimental patterns with the JCPDS powder diffraction file.

Atomic absorption spectroscopy (AAS) was performed with a Perkin–Elmer 2100 Atomic Absorption spectrometer using an air–acetylene flame. Gold/palladium samples were run at wavelengths 242.8 nm (Au) and 247.6 nm (Pd). Samples for analysis were prepared by dissolving 0.1 g of the dried catalyst in an aqua regia solution, followed by the addition of 250 ml deionised water to dilute the sample. AAS was used to determine the wt% of the metal incorporated into the support after impregnation, as well as the concentration (ppm) of Au or Pd that had leached out into solution during reaction, by determin-

ing the Au and Pd content of the used catalyst and comparing with to the fresh catalyst.

Samples for examination by scanning transmission electron microscopy (STEM) were prepared by dispersing the catalyst powder in high-purity ethanol, then allowing a drop of the suspension to evaporate on a holey carbon film supported by a 300-mesh copper grid. Samples were then subjected to chemical microanalysis and annular dark-field imaging in a VG Systems HB603 STEM operating at 300 kV equipped with a Nion C_s corrector. The instrument was also fitted with an Oxford Instruments INCA TEM 300 system for energy-dispersive X-ray (EDS) analysis.

X-Ray photoelectron spectroscopy (XPS) was performed using a VG EscaLab 220i spectrometer, using a standard $\text{Al-K}\alpha$ X-ray source (300 W) and an analyser pass energy of 20 eV. Samples were mounted using double-sided adhesive tape, and binding energies were referenced to the C 1s binding energy of adventitious carbon contamination, which was taken to be 284.7 eV.

3. Results

3.1. Evaluation of Au/TiO₂, Au–Pd/TiO₂, and Pd/TiO₂ calcined catalysts

Titania-supported Au, Pd, and Au–Pd catalysts prepared using impregnation and deposition–precipitation methods were evaluated for the synthesis of H_2O_2 and the oxidation of CO after the catalysts were calcined at 400°C . The results, given in Table 1, demonstrate that deposition–precipitation is the preferred method of preparation of active catalysts for CO oxidation, whereas the best catalysts for H_2O_2 synthesis are prepared by impregnation.

For the catalysts calcined at 400°C prepared by impregnation, the pure Au catalysts all generated H_2O_2 , but at low rates. The addition of Pd to Au significantly enhanced the catalytic performance for the synthesis of H_2O_2 , and it is interesting to note that there was an optimum Pd–Au composition in which the rate of H_2O_2 production was much higher than that for the pure Pd catalyst, which in itself was significantly more active than pure gold. The highest rates are observed for the 2.5 wt% Au/2.5 wt% Pd/TiO₂ catalyst. Furthermore, the rates of hydro-

Table 1
Comparison of hydrogen peroxide productivity and CO conversion for catalysts prepared by deposition–precipitation (DP) and impregnation (I)

Catalyst	Preparation method	Pre-treatment	Productivity ($\text{mol}_{\text{H}_2\text{O}_2} \text{ h}^{-1} \text{ kg}_{\text{cat}}^{-1}$)	H_2O_2 (wt%)	CO conversion (%)
5% Au/TiO ₂ ^a	DP	Air, 25 °C	0.229	0.002	85
5% Au/TiO ₂ ^a	DP	Air, 120 °C	0.482	0.005	76
5% Au/TiO ₂ ^a	DP	Air, 400 °C	0.388	0.004	40
5% Au/TiO ₂ ^a	I	Air, 400 °C	7.1	0.014	<1
4% Au/1% Pd/TiO ₂ ^b	I	Air, 400 °C	28	0.057	<1
2.5% Au/2.5% Pd/TiO ₂ ^b	I	Air, 400 °C	64	0.128	<1
5% Pd/TiO ₂ ^b	I	Air, 400 °C	31	0.061	<1

Reaction conditions as described in text; reaction time for H_2O_2 synthesis 30 min; reaction time for CO oxidation following achievement of steady state: 1–6 h.

Mass of catalyst for H_2O_2 synthesis:

^a 50 mg,

^b 10 mg.

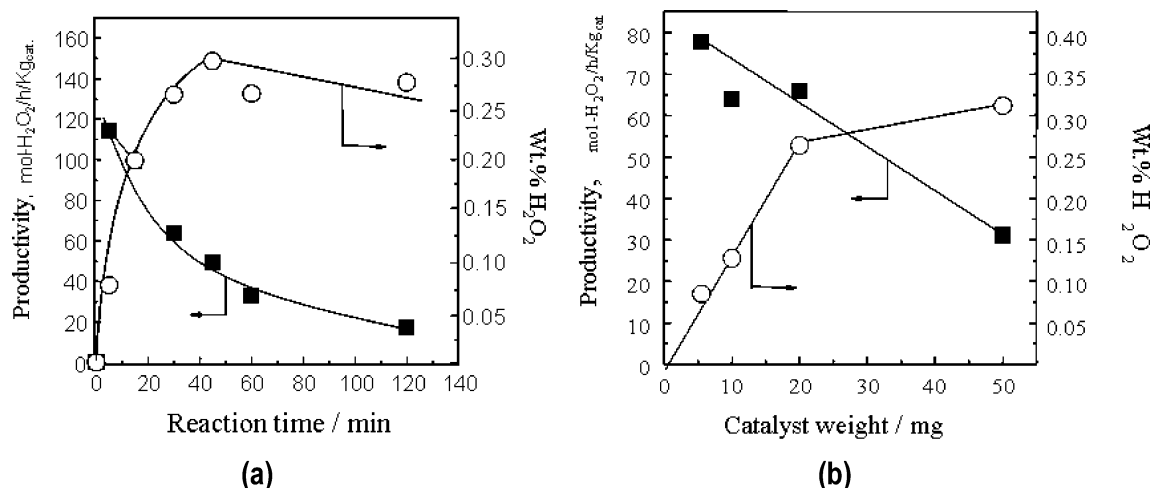


Fig. 1. Effect of (a) reaction time (catalyst mass, 20 mg), and (b) catalyst mass (reaction time, 30 min) on the synthesis of hydrogen peroxide using a 2.5 wt% Au/2.5 wt% Pd/TiO₂ catalyst calcined at 400 °C in air.

Table 2

The influence of reaction time on the conversion of H₂ and selectivity to hydrogen peroxide synthesis^a

Reaction time (min)	Productivity (mol _{H₂O₂} h ⁻¹ kg _{cat} ⁻¹)	H ₂ conversion (%)	H ₂ O ₂ selectivity (%)	H ₂ O ₂ yield (%)
5	114	8	93	7.6
30	66	44	60	26.4
120	17	93	29	27.6

^a 2.5% Au–2.5% Pd/TiO₂ catalyst (20 mg) calcined at 400 °C.

gen peroxide formation with the TiO₂-supported catalysts were generally a factor of three higher than the corresponding Al₂O₃-supported catalysts [28,29], demonstrating that the nature of the support plays an important role in the direct oxidation reaction.

The reaction time and amount of catalyst used are important variables in the direct synthesis reaction, because there are a number of competing processes that lead to the decomposition of hydrogen peroxide, even at 2 °C. The effect of increasing reaction time in the autoclave is shown in Fig. 1a for the 2.5% Au/2.5% Pd/TiO₂ catalyst calcined at 400 °C. Separate experiments were conducted for each reaction time, and so the data indicate the amount of H₂O₂ formed as an average over the reaction period. It is apparent that as the yield of H₂O₂ increased steadily with reaction time, the rate of formation decreased, and we concluded that under our reaction conditions, a reaction time of 30 min provided a reasonable compromise between rate and overall yield of H₂O₂ for comparing the catalytic performance of these catalysts. Of course, the optimal conditions will vary with other conditions, such as temperature and pressure, and so it can be reasonably anticipated that at higher temperatures and reaction pressures, much shorter reaction times will be preferred. This means that the direct synthesis method using diluted reactants, which avoids the potential for explosion hazards, will produce only relatively dilute solutions, and hence the methodology may be better suited to in situ utilisation in chemical syntheses in which the H₂O₂ is used as soon as it is formed. In this scenario, optimum use can be made of the very high initial rates of H₂O₂ formation displayed by the catalysts (Ta-

ble 2). For the 2.5% Au/2.5% Pd/TiO₂ calcined at 400 °C, the initial rate after a 5-min reaction time was >100 mol kg_{cat}⁻¹ h⁻¹ with a hydrogen selectivity of >90%; consequently, if the hydrogen peroxide could be selectively transferred to a substrate, then this process would be exceptionally efficient.

The effect of increasing the amount of catalyst in the autoclave is shown in Fig. 1b for the 2.5% Au/2.5% Pd/TiO₂ calcined at 400 °C. It is apparent that the yield of H₂O₂ increased as the amount of catalyst was increased. However, the rate of H₂O₂ synthesis was highest at lower catalyst masses, and although the rate was linear for catalyst masses up to 20 mg, under our reaction conditions, a catalyst mass of 10 mg provided a reasonable compromise between rate and overall yield of H₂O₂. It is worth noting, however, that catalyst masses of 20 mg can be used effectively, and in cases where the rate is extremely low, we have used a catalyst mass of 50 mg.

3.2. Effect of calcination and reduction

The effect of calcination and reduction on the optimum composition of the TiO₂-supported catalyst was investigated; the results are presented in Table 3. It is apparent that calcination either by itself or followed by reduction in H₂ led to a significant decrease in the rate of H₂O₂ synthesis, determined as an average over the 30-min reaction period. An extensive study of the effect of calcination of the 2.5% Au/2.5% Pd/TiO₂ catalyst showed that the rate of H₂O₂ synthesis (Fig. 2a) and H₂ selectivity (as measured by the yield of H₂O₂) were both particularly sensitive to this preparation parameter (Fig. 2b). In addition, the duration of catalyst drying can also significantly affect performance (Fig. 3a).

The uncalcined sample (i.e., a sample dried only at 25 °C) gave the highest rate of H₂O₂ synthesis (202 mol_{H₂O₂} h⁻¹ kg_{cat}⁻¹), H₂ conversion (46%), and H₂O₂ selectivity (89%). This represents the highest rate based on catalyst mass observed to date with any Au- or Pd-based catalyst for the direct synthesis of H₂O₂. The selectivity is notably higher than the values that we have reported previously [28,29] for Au–Pd/Al₂O₃ cat-

Table 3
The effect of catalyst calcination and/or reduction treatment on H₂O₂ synthesis^a

Catalyst	Pretreatment	Productivity (mol _{H₂O₂} h ⁻¹ kg _{cat} ⁻¹)	H ₂ O ₂ (wt%)	H ₂ conversion (%)	H ₂ O ₂ selectivity (%)
2.5% Pd/TiO ₂	Air, 25 °C	90	0.180	38	48
5% Pd/TiO ₂	Air, 25 °C	173	0.346	86	40
2.5% Au–2.5% Pd/TiO ₂	Air, 25 °C	202	0.404	46	89
5% Pd/TiO ₂	Air, 200 °C, 3 h	99	0.198	42	47
2.5% Au–2.5% Pd/TiO ₂	Air, 200 °C, 3 h	124	0.248	34	73
2.5% Pd/TiO ₂	Air, 400 °C, 3 h	24	0.048	19	25
5% Pd/TiO ₂	Air, 400 °C, 3 h	31	0.062	29	21
2.5% Au–2.5% Pd/TiO ₂	Air, 400 °C, 3 h	64	0.128	21	61
2.5% Au–2.5% Pd/TiO ₂	Air, 400 °C, 3 h + H ₂ 500 °C	32	0.064	nd	nd

^a Reaction time 30 min; mass of catalyst 10 mg; nd, not determined.

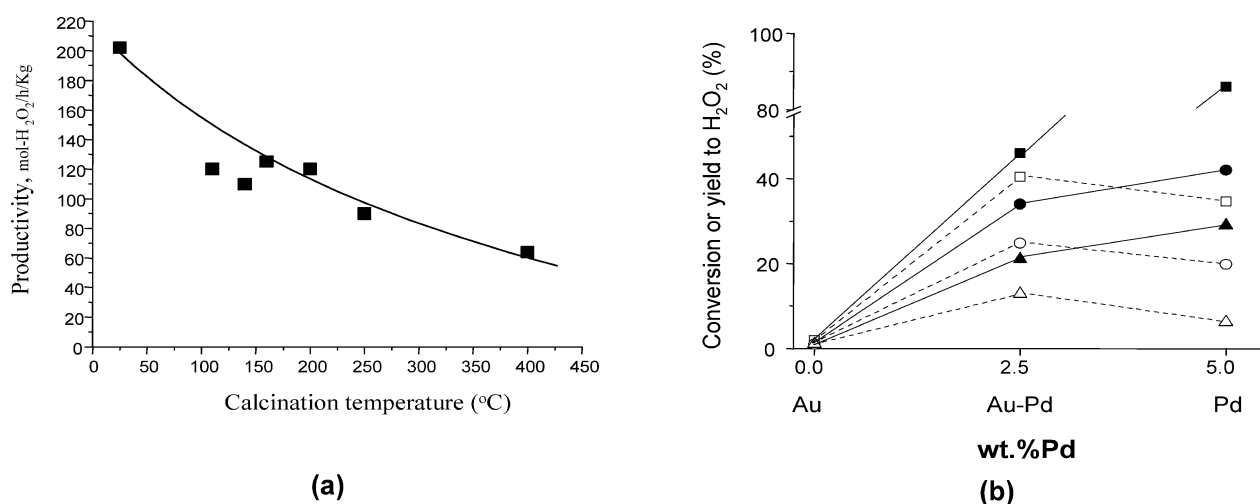


Fig. 2. (a) Influence of the calcination temperature of 2.5 wt% Au–2.5 wt% Pd/TiO₂ catalysts on the productivity to hydrogen peroxide. Reaction time is 30 min, and reaction conditions are as described in the text. (b) H₂ conversion (■, ●, ▲) and H₂O₂ yield (□, ○, △) obtained for Au, Au–Pd and Pd/TiO₂ catalysts. Symbols: uncalcined (■, □), calcined in air at 200 °C (●, ○) and calcined in air at 400 °C (▲, △).

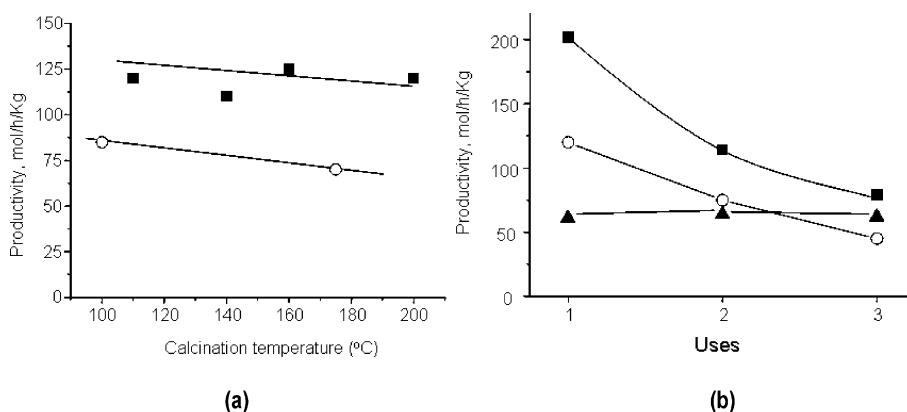


Fig. 3. (a) Influence of the drying time of 2.5 wt% Au–2.5 wt% Pd/TiO₂ catalysts prior to calcination on the productivity to H₂O₂. Symbols: (■) dried for 3 h, (○) dried for 16 h. Reaction conditions as described in the text. (b) The effect of the number of uses on the productivity for H₂O₂ formation for a series of 2.5 wt% Au–2.5 wt% Pd/TiO₂ catalysts. Symbols: uncalcined (■), calcined in air at 200 °C (●) and calcined in air at 400 °C (▲).

alysts, and also for Pd catalysts. For example, Choudhary et al. [30,31] obtained selectivities to H₂O₂ of 85 and 72% at H₂ conversions of 21 and 9% using Pd/Ga₂O₃ and Pd/H-ZSM-5 catalysts, respectively.

3.3. Catalyst stability

A key factor that must be considered for heterogeneous catalysts operating in three-phase systems is the possibility that ac-

Table 4
Leaching of gold and palladium in 2.5% Au–2.5% Pd/TiO₂ catalysts after reaction

Pre-treatment	Run	Loss of Au ^a (%)	Loss of Pd ^a (%)
Air, 25 °C	1	80	90
	2	92	95
Air, 200 °C, 3 h	1	11	0
	2	13	0
Air, 400 °C, 3 h	1	0	0
	2	0	0

^a ((Au or Pd in fresh catalyst) – (Au or Pd after run 1 or 2))/(Au or Pd in fresh catalyst) × 100.

tive components can leach into the reaction mixture, leading to catalyst deactivation or, in the worst case, to the formation of an active homogeneous catalyst [32]. The high-activity uncalcined Au–Pd/TiO₂ catalysts were, unfortunately, particularly unstable and deactivated significantly with successive uses (Fig. 3b). AAS analysis revealed that almost all of the Au and Pd were lost during the initial use. Table 4 shows the loss of palladium and gold by leaching after catalytic testing for the following 2.5% Au/2.5% Pd/TiO₂ catalysts: uncalcined, calcined at 200 °C, and calcined at 400 °C. The catalyst calcined at 400 °C did not leach either Au or Pd within the limits of detection, and did not deactivate with reuse (Fig. 3b). However, the catalysts that were either uncalcined or calcined at 200 °C lost both gold and palladium after reaction (Table 4) and showed a consequent decrease in activity in subsequent reuse tests (Fig. 3b). It should be noted that the loss of metals by leaching was proportionately much larger than the expected decrease in productivity for hydrogen peroxide formation. The absence of leaching of either Au or Pd from the catalysts calcined at 673 K, as determined by AA and XPS, suggests that these materials function as wholly heterogeneous catalysts.

3.4. Catalyst characterisation

To determine the nature of the supported Au–Pd catalysts, a detailed structural and chemical characterisation was carried out using STEM and XPS. The catalysts all had total BET surface areas in the range 35–45 m² g⁻¹, and this was not considered an important factor with respect to activity. The catalysts were also characterised using powder XRD; these spectra are provided as supplementary data.

3.4.1. XPS characterisation

Fig. 4 shows the combined Au 4d and Pd 3d spectra for a 2.5 wt% Au/2.5 wt% Pd/TiO₂ catalyst after different heat treatments. For the uncalcined sample, which exhibited the highest rate of H₂O₂ production that we have observed to date for a titania-supported catalyst, there were clear spectral contributions from both Au and Pd, leading to severe overlap of peaks. After heat treatment at 200 °C, there was a dramatic decrease in the intensity of the Au 4d peaks, and after calcination in air at 400 °C followed by reduction in H₂ at 500 °C, the intensity of the Au 4d_{3/2} feature was below detection limits. To quantify the surface composition of the uncalcined catalyst, we needed to deconstruct the spectral envelope into its respective Pd 3d and

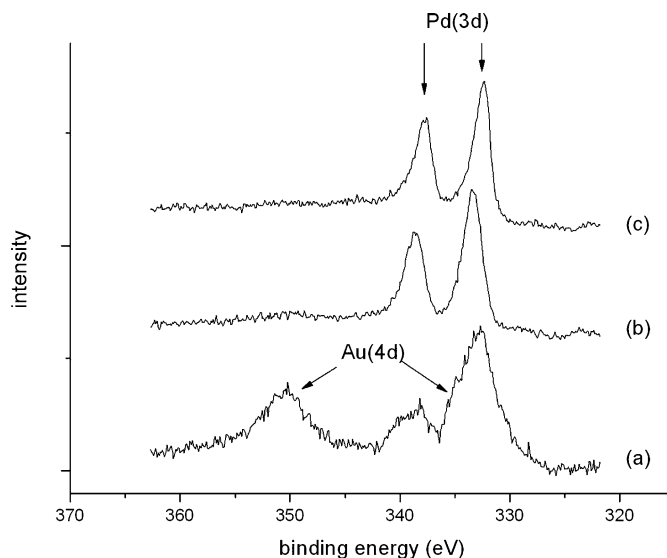


Fig. 4. Au 4d and Pd 3d spectra for a 2.5 wt% Au–2.5 wt% Pd/TiO₂ catalyst after different heat treatments: (a) uncalcined, (b) calcined at 200 °C in air, (c) calcined at 400 °C in air and 500 °C in hydrogen.

Au 4d components. This was best achieved by subtracting out the Pd 3d contribution, using a suitably scaled and shifted reference spectrum. Although the calcined and reduced sample can provide such a standard in principle, it is clear from a visual inspection that the FWHM of the Pd 3d_{3/2} peak was much greater in the uncalcined spectrum; this may be due in part to the fact that palladium was present as both Au–Pd alloy particles and pure Pd particles, as observed in the TEM measurements (qv. post). In fact, a suitable Pd reference spectrum is provided by an uncalcined Au (1 wt%)-Pd (4 wt%)/Al₂O₃ sample, which is shown in Fig. 5 together with the Au 4d + Pd 3d spectrum for the uncalcined 2.5 wt% Au/2.5 wt% Pd/TiO₂ sample and the Au 4d spectrum obtained by subtraction of the scaled Pd 3d spectrum. From the resulting Au 4d and Pd 3d peak areas, and making use of the sensitivity factors provided by Wagner [33], we calculated the Pd:Au ratio to be 1:2.9 by weight, suggesting, on average, a significant surface enrichment by gold in the uncalcined sample. AAS confirmed an overall Au:Pd ratio of 1:1, although as the TEM results showed (qv. post), this simple ratio masks a very complex microstructure. The spectra observed for the uncalcined sample after reaction (Fig. 6) were consistent with the substantial leaching of metal into solution observed in the catalytic studies, demonstrating weak Pd features and no detectable gold intensity.

In dramatic contrast to the uncalcined sample, the catalyst calcined at 200 °C exhibited a Pd/Au ratio (by weight) of 5.1:1 from XPS analysis. Because AAS and XEDS analysis showed the composition of the catalysts were as was expected from the preparation, viz. a ratio of 1:1 by weight, the XPS results are consistent with the development of a core–shell structure for the metal particles (gold core–palladium shell) on the catalyst after heat treatment. The photoelectron flux emitted from the gold atoms in the core was strongly attenuated due to inelastic scattering of the electrons during transport through the Pd shell, leading to a significantly reduced Au signal intensity compared

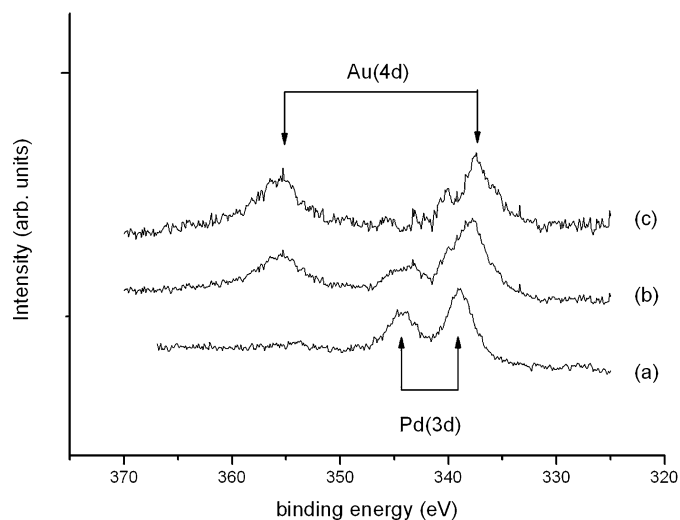


Fig. 5. Extraction of the Au 4d components (curve (c)) from the composite Au–Pd spectrum (b), for a fresh uncalcined 2.5 wt% Au–2.5 wt% Pd/TiO₂ catalyst, by subtracting a reference Pd 3d spectrum (a) recorded for an uncalcined Au (1.0 wt%)-Pd (4.0 wt%)/Al₂O₃ sample.

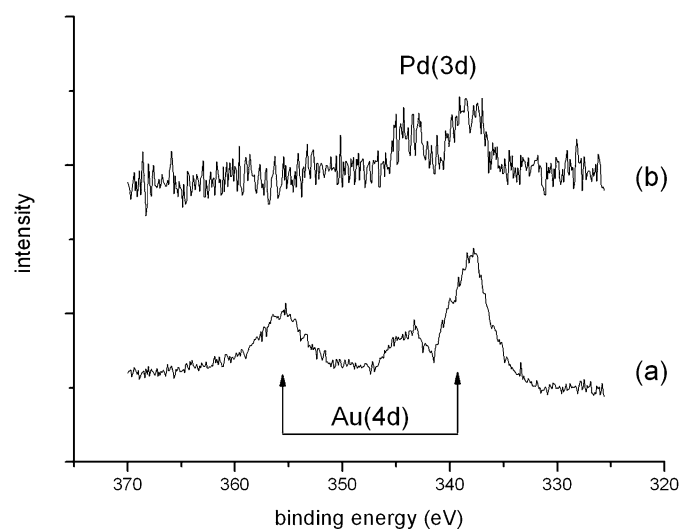


Fig. 6. Au 4d and Pd 3d spectra for an uncalcined 2.5 wt% Au–2.5 wt% Pd/TiO₂ catalyst (a) before and (b) after reaction.

with Pd. A similar enrichment has been observed [34] for bulk Pd–Au alloys heated in oxygen at temperatures $>300^{\circ}\text{C}$, in which the surface layer is known to consist of PdO. Thermodynamically, this is a consequence of the exothermic heat of formation of PdO compared with the endothermic heat of formation of Au₂O₃. Interestingly, it was also found that hydrogen treatment at 350°C resulted in the complete reduction of the oxide without re-equilibration of the surface composition to that of the bulk [34], as was also observed in the present study (Fig. 4).

Both the high Pd/Au ratio and the dramatic decrease in the Au signal on calcination at 673 K are indicative of core–shell particles. This phenomenon may be partly explained by the loss of small Au particles as revealed by STEM-XEDS (qv. post), but there is no evidence of the development of massive Au particles after calcination. The presence of small Pd particles

identified in STEM-XEDS after calcination (qv. post) are not relevant in this context, because the Pd atoms that form these particles must have been present on the uncalcined sample and thus contributed to the observed Pd signal in both cases. The large observed increase in the Pd/Au ratio is consistent with the attenuation of the Au signal by Pd overlayers.

The formation of Au–Pd core–shell structures has been reported previously for ligand-stabilized bimetallic Au–Pd colloids [35] and in the preparation of bimetallic nanoparticles by the sonochemical reduction of solutions containing gold and palladium ions [36]. Such core–shell particles were found to exhibit superior catalytic activity compared with Au–Pd alloy particles exhibiting the same overall Au/Pd ratio [36]. Detailed ¹⁹⁷Au Mössbauer measurements have confirmed the presence of a pure Au core and also identified a thin alloy region at the interface between the Au core and the Pd shell [36,37]. Inverted Pd core/Au shell particles may be prepared, but with difficulty [38]; even if Au is deposited on already-formed Pd particles, Au core/Pd shell structures are formed [39]. Interestingly, the core–shell particles reported in our study are stable at temperatures up to at least 500°C , in contrast to core–shell nanoparticles prepared ultrasonically in a porous silica support, where transformation to a random alloy was observed at 300°C [40].

The transformation of the Pd 3d peak shapes from broad and symmetric in the sample calcined in air at 200°C to sharp but asymmetric in the sample calcined in air at 400°C then reduced in H₂ at 500°C , together with a shift to lower binding energy by 0.8 eV , is consistent with the reduction of Pd^{δ+} to Pd⁰.

3.5. STEM characterisation

Annular dark field (ADF) STEM images of the uncalcined Au–Pd/TiO₂ (2.5% Au/2.5% Pd) catalyst revealed a bimodal metal particle size distribution. The smaller particles ranged from approximately 1 to 8 nm, with most of the particles at the lower end of this range. In contrast, the larger particles ranged from 40 to 70 nm in diameter but were definitely the minority phase. STEM-XEDS mapping analysis revealed the coexistence of at least three types of metal particles, as shown in Fig. 7.

Most of the smaller particles were pure Au; only a very small fraction was pure Pd. In contrast, all of the larger particles were Au–Pd alloys, as evidenced by the spatial coincidence of the gold and palladium X-ray maps. A minority of the smaller particles also contained both gold and palladium, as shown in Fig. 8. Also of note in this image is the presence of very small metal particles ($<1\text{ nm}$) that were not identified by XEDS because of the extremely poor X-ray signal that they emitted but were clearly resolved via z-contrast HAADF imaging.

For the calcined Au–Pd/TiO₂ sample, a similar bimodal metal particle size distribution was found. In this case, however, the smaller particle size distribution was slightly larger than that in the uncalcined sample (2–10 nm), whereas most of the larger particles were 35–80 nm in size. A few isolated particles even exceeded 120 nm in diameter. Chemical microanalysis via STEM-XEDS of the calcined sample once again revealed that the larger particles all consisted of Au–Pd alloys

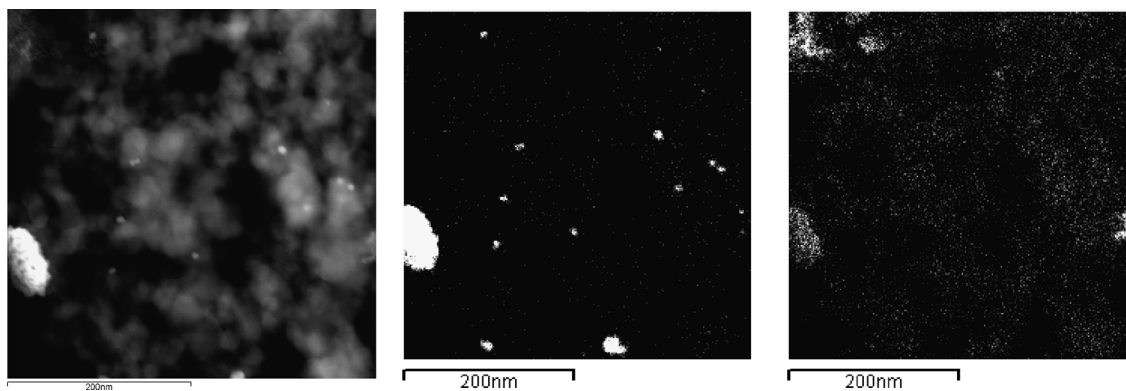


Fig. 7. HAADF image (left) of 2.5 wt% Au–2.5 wt% Pd/TiO₂ uncalcined sample and corresponding XEDS maps of Au-M₂ (centre) and Pd-L₁ (right); note the presence of pure-Au, pure-Pd, and larger Au–Pd alloy particles.

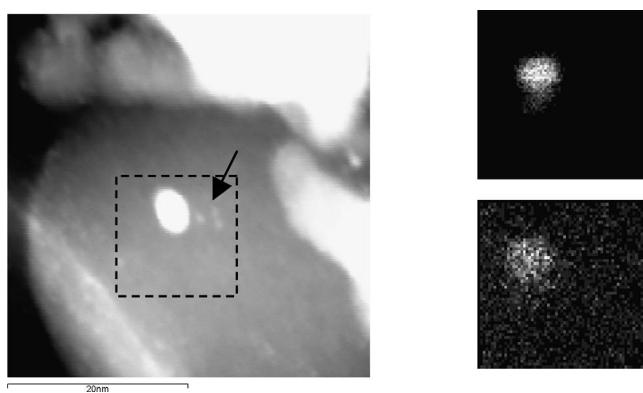


Fig. 8. ADF-STEM image showing small alloy particle in uncalcined 2.5 wt% Au–2.5 wt% Pd/TiO₂ sample (left); reduced raster Au-M₂ map (top right), and Pd-L₁ map (lower right); the arrow indicates a group of even smaller particles which could not be identified by XEDS.

(Fig. 9). However, in marked contrast to the uncalcined catalyst, all of the smaller particles observed consisted entirely of pure Pd (Fig. 10).

No pure Au particles or small alloy particles were observed in this calcined catalyst. XEDS maps of the larger particles showed that the Au-M₂ (9.712 keV) and the Pd-L_α (2.838 keV) signals were spatially coincident, indicating that the metal nanoparticles in the field of view were in fact Au–Pd alloys. Closer inspection of the larger alloy particle in Fig. 9 shows a

definite discrepancy between the spatial extent of the Au and Pd signals; that is, the Pd X-ray signal always originated from a larger area than the corresponding gold signal. This suggests a tendency for Pd surface segregation in these alloy particles, as indicated by the XPS analysis (qv.).

A morphological feature unique to the calcined titania catalyst is shown in Fig. 11. In addition to the large, rounded Au–Pd alloy particles, a few metal particles with a nanorod morphology were also found. STEM-XEDS mapping showed that these nanorods have a similar alloy composition to the other more spherical particles and also characteristically had a Pd-signal originating from a larger spatial area than the Au-signal, due once again to Pd surface segregation.

Comparing the calcined and uncalcined catalysts, the most striking difference was the composition of the smaller particles in each. Although both contained small palladium particles, only the uncalcined sample exhibited any pure gold particles. Indeed, we did not find pure gold particles in our previous studies of the alumina-supported catalysts [28,29]. This observation suggests that the chemical composition of the metal particles in these catalysts is strongly influenced by the heat treatment process used. It is also interesting to note the presence of a very few large (≈70 nm) metal particles in this uncalcined sample (see Fig. 7). This suggests that either these large particles are a direct byproduct of the impregnation synthesis process or they

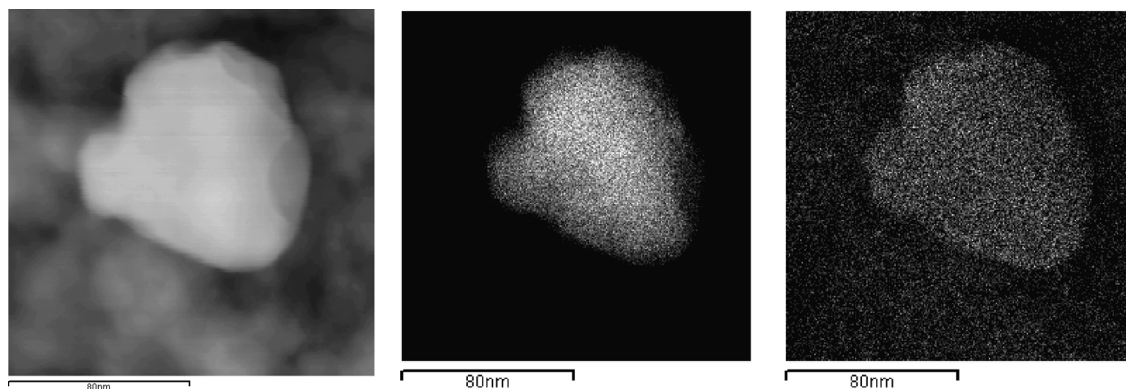


Fig. 9. STEM-ADF image of 2.5 wt% Au–2.5 wt% Pd/TiO₂ catalyst calcined at 400 °C, showing large alloy particle (left), Au-M₂ STEM-XEDS map (centre), Pd-L₁ STEM-XEDS map (right); note that the Pd signal appears to originate from a larger area than that of the Au signal.

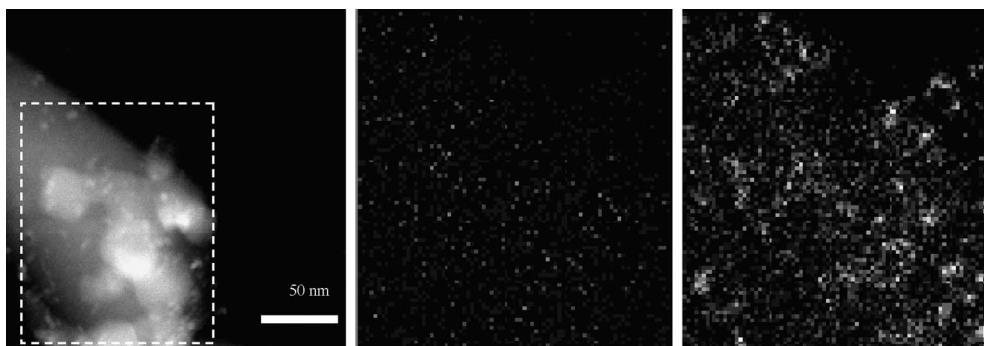


Fig. 10. HAADF images showing small Pd particles in the calcined 2.5 wt% Au–2.5 wt% Pd/TiO₂ (left), reduced scan area Au-M₂ map (centre), and Pd-L₁ map (right).

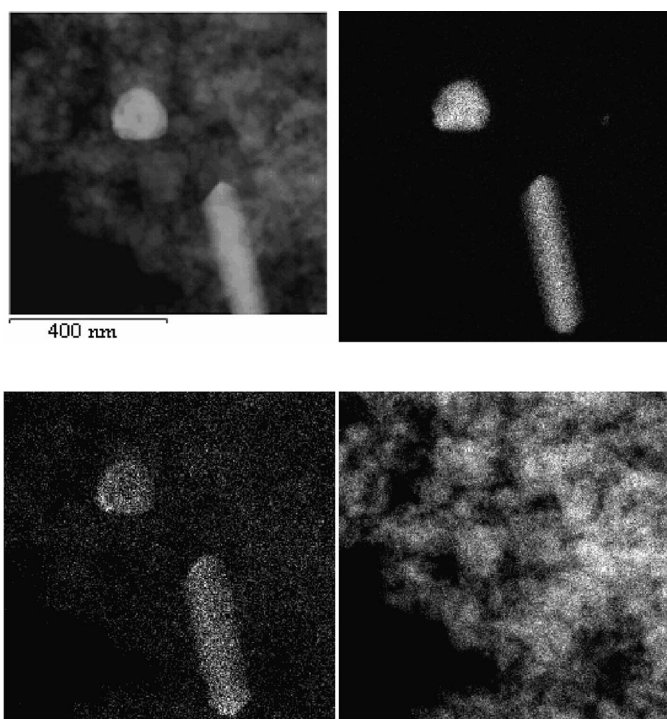


Fig. 11. ADF image (top left) of 2.5 wt% Au–2.5 wt% Pd/TiO₂ sample and corresponding XEDS maps of Au (top right), Pd (bottom left), and Ti (bottom right); note that the Pd signal appears to originate from a larger spatial area than the Au signal in both the spherical and rod-like particles.

form over time even in the absence of elevated-temperature calcination.

Our observations suggest that on heat treatment, the smaller pure-Au particles sinter and combined with palladium to form the large alloy particles discussed earlier. The origin of the large population of small pure-Pd particles after this heat treatment remains unclear. One possible explanation is that there was a significant concentration of palladium in the uncalcined sample that was atomically dispersed (and was not detected by the STEM investigation) and that aggregated to larger particles on heat treatment. Another possibility is that the small palladium particles already existed in the uncalcined catalyst but did not bind well to the titania particles and were leached off during wet preparation of the STEM sample using ethanol.

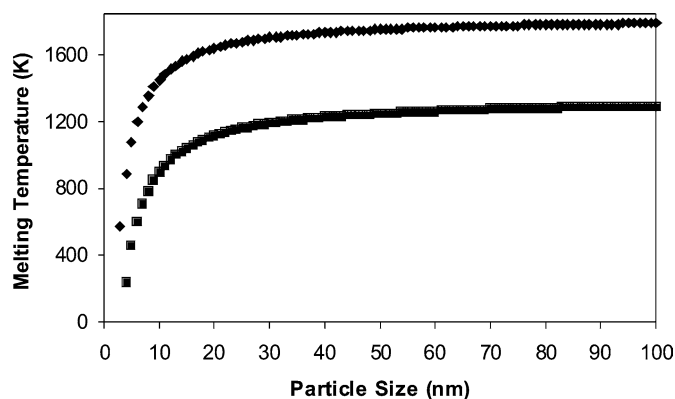


Fig. 12. Melting point as a function of particle size for palladium and gold; note that in the 5 nm range the melting point of gold (■) is significantly lower than that of palladium (◆).

It is a well-established phenomenon that as the radius of metal particles is reduced to approximately 10 nm, the melting point of that metal is lowered significantly below the value exhibited by the bulk metal. Using the equation developed by Buffat et al. [41], a plot can be drawn for the melting point of gold and palladium as a function of particle size, as shown in Fig. 12. Clearly, the drying temperature (120 °C) and the calcination temperature (400 °C) were both a much higher fraction of the melting point of gold than that of palladium in the region where the particle radius was <5 nm. This may explain the presence of pure Pd and the lack of pure Au particles in the calcined sample, because the less refractory Au ($T_m(\text{bulk}) = 1337 \text{ K}$) would have a significantly higher atomic mobility than that of the Pd ($T_m(\text{bulk}) = 1828 \text{ K}$). The increased mobility of the gold relative to the palladium would result in it being incorporated into the larger particles (as we have observed), whereas the palladium would need significantly more time to sinter to this same degree. The presence of gold nanoparticles in the 120 °C dried sample and the possible retention of atomically dispersed palladium could also be explained by this strong difference in mobility between the Au and Pd nanoclusters at this drying temperature.

The strong tendency for palladium surface segregation, observed in this study and for bulk alloys [34], was not expected. This was presumably brought about by the preferential forma-

tion of Pd–O bonds at the alloy surface, because palladium oxidizes more readily than gold in this temperature range.

3.6. XRD results

The XRD results (Fig. 2 in the [supporting information](#)) are in agreement with the XPS and STEM data. XRD analysis of the uncalcined catalyst showed no Au signal, in keeping with the STEM conclusion that the gold was present mainly as small particles. Calcination led to the development of large alloy particles, as evidenced in the XRD results by the appearance of a signal characteristic of Au/Au–Pd species.

4. Discussion

The results that we present here for Au–Pd/TiO₂ catalysts for the direct synthesis of H₂O₂ are the most significant reported to date for this important reaction. In particular, the initial rates determined after a short reaction time in the autoclave for the Au–Pd/TiO₂ catalyst calcined at 400 °C are the highest yet published (114 mol_{H₂O₂} h⁻¹ kg_{cat}⁻¹, H₂ conversion 8%, and H₂O₂ selectivity 93%) for a stable heterogeneous catalyst. The uncalcined sample (i.e., a sample dried at 25 °C) gives a much higher rate at comparable selectivity at 30 min reaction time (202 mol_{H₂O₂} h⁻¹ kg_{cat}⁻¹, H₂ conversion 45.5%, and H₂O₂ selectivity 89%), but unfortunately this catalyst rapidly loses gold and palladium into solution and cannot be effectively reused. In contrast, the calcined catalyst can be reused many times without loss of performance.

We have obtained these results using a stirred autoclave as the reactor. However, we believe that the results show considerable promise in that, using an appropriately designed flow reactor, these Au–Pd catalysts should be able to produce H₂O₂ at rates and selectivities appropriate for commercialisation. Two scenarios can be envisaged. First, the stable calcined catalysts could be used at short contact time in a suitable flow reactor to generate H₂O₂ at high selectivity (based on H₂), which could either be captured by absorption or reacted in situ with appropriate substrates. We are currently investigating this strategy as part of our studies. Second, the higher rates obtained with high selectivity for the uncalcined material are intriguing. It is possible that these uncalcined catalysts can form the basis for a gas phase process operated at low temperature, because leaching of Au and Pd might be eliminated when using gas phase reactants; we will be investigating this possibility.

The origin of the catalytic activity is not yet clear from our studies with the uncalcined materials. It could arise from a number of possibilities, including (a) active surface-bound metallic particles that are subsequently dissolved, with an inactive solution species; (b) release of small colloidal particles into the solvent that display high activity; and/or (c) the solution form of the leached metal being the active component. We have not been able to distinguish between these three mechanisms; indeed, all three may be operative, because at the end of the experiment in the autoclave no gold or palladium remained in solution, and so the colloidal particles or soluble species must

have been rapidly deposited onto the autoclave and stirrer. Numerous blank experiments have shown that this deposited form of metal is inactive. Lunsford [42,43] showed that colloidal Pd is very active for H₂O₂ synthesis and indeed can play a role in many of the previous Pd-catalysed reactions. Hence it is possible that the high activities that we observed with uncalcined catalysts may be due to the generation of colloidal metallic particles that are both highly efficient catalysts and short-lived. Moreover, it is clear from our characterisation studies that the uncalcined samples are the most complex structurally.

The nature of the active site for the direct synthesis of H₂O₂ is clearly different from the active site for low-temperature CO oxidation, as evidenced by the data that we have presented showing that the catalysts that are effective for H₂O₂ synthesis are inactive for CO oxidation, and vice versa. We have made a more extensive study of this inverse relationship and have found that it holds for all of the supports we have investigated to date (TiO₂, Al₂O₃, SiO₂, Fe₂O₃, and C). This is an important observation, because the reaction of H₂ represents a selective, or partial, oxidation, whereas the reaction of CO can be considered a total oxidation process. The mechanism of CO oxidation on supported Au catalysts also remains the subject of intense interest, the catalysis having been variously attributed to gold nanoclusters with size-dependent electronic properties [44] and chemical properties [45,46] compared with bulk gold, low-coordinated gold atoms in nanoclusters [47], and surface defects of the support [48]. Recently, evidence for the role of gold cations in the water gas shift reaction was provided by Flytzani–Stephanopoulos [49] and Guzman and Gates [50]. Furthermore, in an elegant model study of high activity Au/TiO₂ model catalysts, Goodman [51] proposed that activity in this system is associated solely with metallic gold atoms. However, as noted by Haruta [52], the evidence with respect to the mechanism for real highly dispersed gold catalysts tends to point toward the importance of cationic gold species, perhaps at the peripheral sites where the gold nanoparticles come in direct contact with the support and the gaseous reactant species. The situation is therefore complex, and as yet there is no consensus except that small gold nanoclusters, possibly comprising cationic gold, are probably associated with the high activity. In the case of the calcined Au/TiO₂ catalysts prepared by impregnation and used in the present study, the gold particles were larger than is considered optimal for CO oxidation, and consequently we consider that relatively large Au nanocrystals are active for the selective oxidation of H₂. Interestingly, we have also observed that large Au nanocrystals (ca. 25 nm) are very selective for the oxidation of glycerol to glycerate [53,54] and the preferential oxidation of CO in the presence of H₂ [55]. Hence selective oxidations with Au catalysts require a significantly different microstructure than the catalysts that are most active for CO oxidation.

In the present study, a synergistic effect was clearly observed for the addition of Pd to Au for the TiO₂-supported catalysts that was similar in magnitude to that observed with Al₂O₃ as a support [28,29]. The active catalysts contained relatively large alloy particles with a Au core surrounded by a Pd-rich shell, although we cannot determine at this stage whether all or part

of the observed activity is related to these structures. However, it is likely that the high activity and high selectivity sites for H₂ oxidation are significantly different from those in the pure Au/TiO₂ catalysts.

5. Conclusions

We have shown that calcined Au–Pd/TiO₂ materials are highly effective catalysts for the direct synthesis of H₂O₂ from the oxidation of H₂, and very high rates and selectivities can be achieved (114 molH₂O₂ h⁻¹ kg_{cat}⁻¹ and H₂O₂ selectivity 93%) under appropriate conditions. These catalysts are stable and can be reused as long as they are calcined at 400 °C before initial use. Pretreatment at lower temperatures leads to an unstable, but even more active, catalyst. In conclusion, these results provide the basis for the commercial design of a direct synthesis process that can be performed outside of the explosive region and hence can provide safe and efficient synthesis of H₂O₂.

Acknowledgments

This work formed part of the EU AURICAT project (Contract HPRN-CT-2002-00174) and the EPSRC/Johnson Matthey-funded ATHENA project. The authors thank the World Gold Council (through the GROW scheme), and Cardiff University (AA Reed studentship) for providing support for J.K.E., C.J.K., and A.H. also acknowledge the generous support of the NSF Materials Research Science and Engineering Center (NSF DMR-0079996).

Supporting information

Supporting information associated with this article can be found, in the online version, at [doi:10.1016/j.jcat.2005.09.015](https://doi.org/10.1016/j.jcat.2005.09.015).

References

- [1] R.A. Sheldon, *Stud. Surf. Sci. Catal.* 66 (1991) 573.
- [2] M. Besson, P. Gallezot, *Catal. Today* 57 (2000) 127.
- [3] D. Enders, L. Wortmann, R. Peters, *Acc. Chem. Res.* 33 (2000) 157.
- [4] A.R.J. Vaino, *Org. Chem.* 65 (2000) 4210.
- [5] S. Lee, P.L. Fuchs, *J. Am. Chem. Soc.* 124 (2002) 13978.
- [6] P. Wadhvani, M. Mukherjee, D. Bandyopadhyay, *J. Am. Chem. Soc.* 123 (2001) 12430.
- [7] P.B. Walsh, *Tappi J.* 74 (1991) 81.
- [8] M. Taramasso, G. Peego, B. Notari, US Patent 4410501 (1983).
- [9] H.T. Hess, in: I. Kroschwitz, M. Howe-Grant (Eds.), *Kirk–Othmer Encyclopedia of Chemical Engineering*, vol. 13, Wiley, New York, 1995, p. 961.
- [10] H. Henkel, W. Weber, US Patent 1108752 (1914).
- [11] G.A. Cook, US Patent 2368640 (1945).
- [12] Y. Izumi, H. Miyazaki, S. Kawahara, US Patent 4009252 (1977).
- [13] Y. Izumi, H. Miyazaki, S. Kawahara, US Patent 4279883 (1981).
- [14] H. Sun, J.J. Leonard, H. Shalit, US Patent 4393038 (1981).
- [15] L.W. Gosser, J.-A.T. Schwartz, US Patent 4772458 (1988).
- [16] L.W. Gosser, US Patent 4889705 (1989).
- [17] C. Pralins, J.-P. Schirmann, US Patent 4996039 (1991).
- [18] T. Kanada, K. Nagai, T. Nawata, US Patent 5104635 (1992).
- [19] J. van Weynbergh, J.-P. Schoebrechts, J.-C. Colery, US Patent 5447706 (1995).
- [20] S.-E. Park, J.W. Yoo, W.J. Lee, J.-S. Chang, U.K. Park, C.W. Lee, US Patent 5972305 (1999).
- [21] G. Paparatto, R. d'Aloisio, G. De Alberti, P. Furlan, V. Arca, R. Buzzoni, L. Meda, EP Patent 0978316A1 (1999).
- [22] B. Zhou, L.-K. Lee, US Patent 6168775 (2001).
- [23] M. Nystrom, J. Wangangrd, W. Herrmann, US Patent 6210651 (2001).
- [24] J.W. Hastie, *Chem. Phys. Lett.* 17 (1972) 195.
- [25] S.E. Park, L. Huang, C.W. Lee, J.-S. Chang, *Catal. Today* 61 (2000) 117.
- [26] E.D. Park, Y.-S. Huang, J.S. Lee, *Catal. Commun.* 2 (2001) 187.
- [27] R. Meiers, U. Dingerdissen, W.F. Hölderich, *J. Catal.* 176 (1998) 376.
- [28] P. Landon, P.J. Collier, A.J. Papworth, C.J. Kiely, G.J. Hutchings, *Chem. Commun.* (2002) 2058.
- [29] P. Landon, P.J. Collier, A.J. Papworth, C.J. Kiely, G.J. Hutchings, A. Burrows, *Phys. Chem. Chem. Phys.* 5 (2003) 1917.
- [30] V.R. Choudhary, A.G. Gaikwad, S.D. Sansare, *Catal. Lett.* 83 (2002) 235.
- [31] V.R. Choudhary, A.G. Gaikwad, S.D. Sansare, *Catal. Lett.* 84 (2002) 81.
- [32] R.A. Sheldon, I. Arends, G.-J.T. Brink, A. Dijkstra, *Acc. Chem. Res.* 35 (2002) 774.
- [33] C.D. Wagner, L.E. Davis, M.V. Zeller, J.A. Taylor, R.M. Raymond, L.H. Gale, *Surf. Interface Anal.* 3 (1981) 211.
- [34] A. Hilaire, P. Legare, Y. Holl, G. Maire, *Surf. Sci.* 103 (1981) 125.
- [35] A.F. Lee, C.J. Baddeley, C. Hardacre, M.R. Ormerod, R.M. Lambert, G. Schmid, H.J. West, *Phys. Chem.* 99 (1995) 6096.
- [36] H. Takatani, H. Kago, Y. Kobayashi, F. Hori, R. Oshima, *Trans. Mater. Res. Soc. Japan* 28 (2003) 871.
- [37] Y. Kobayashi, S. Kiao, M. Seto, H. Takatani, M. Nakanishi, T. Oshima, *Hyperfine Interact.* 156/157 (2004) 75.
- [38] H. Takatani, F. Hori, M. Nakanishi, R. Oshima, *Australia J. Chem.* 53 (2003) 1025.
- [39] C. Kan, W. Cai, C. Li, L. Zhang, H.J. Hofmeister, *J. Phys. D* 36 (2003) 1609.
- [40] T. Nakagawa, H. Nitani, S. Tanabe, K. Okitsu, S. Seino, Y. Mizukoshi, T.A. Yamamoto, *Ultrason. Sonochem.* 12 (2004) 249.
- [41] P. Buffat, *Thin Solid Films* 32 (1970) 283.
- [42] D. Dissanayake, J. Lunsford, *J. Catal.* 206 (2002) 173.
- [43] D. Dissanayake, J. Lunsford, *J. Catal.* 214 (2003) 113.
- [44] M. Valden, X. Lai, D.W. Goodman, *Science* 281 (1998) 1647.
- [45] D.C. Maeir, D.W. Goodman, *J. Am. Chem. Soc.* 126 (2004) 1892.
- [46] V.A. Bondzie, S.C. Parker, C.T. Campbell, *Catal. Lett.* 63 (1999) 143.
- [47] N. Lopez, J.K. Nørskov, *J. Am. Chem. Soc.* 124 (2002) 11262.
- [48] G.C. Bond, D.T. Thompson, *Gold Bull.* 33 (2000) 41.
- [49] Q. Fu, H. Saltsburg, M. Flytzani-Stephanopoulos, *Science* 301 (2003) 935.
- [50] J. Guzman, B.C. Gates, *J. Phys. Chem. B* 106 (2002) 7659.
- [51] M.S. Chen, D.W. Goodman, *Science* 306 (2004) 252.
- [52] M. Haruta, *Gold Bull.* 37 (2004) 27.
- [53] S. Carrettin, P. McMorn, P. Johnston, K. Griffin, G.J. Hutchings, *Chem. Commun.* (2002) 696.
- [54] S. Carrettin, P. McMorn, P. Johnston, K. Griffin, G.J. Hutchings, C.J. Kiely, *J. Phys. Chem. Chem. Phys.* 5 (2003) 1329.
- [55] P. Landon, J. Ferguson, B.E. Solsona, T. Garcia, A.F. Carley, A.A. Herzog, C.J. Kiely, S.E. Golunski, G.J. Hutchings, *Chem. Commun.* (2005) 3385–3387.